Available online at www.sciencedirect.com
ScienceDirect
Surface & Coatings Technology 202 (2007) 648–652
SURFACE & COATINGS TECHNOLOGY
www.elsevier.com/locate/surfcoat

Adhesion energy of a YPSZ EB-PVD layer in two thermal barrier coating systems

P.-Y. Théry [a,*], M. Poulain [a], M. Dupeux [b], M. Braccini [b]

[a] ONERA-DMMP, 29 avenue de la division Leclerc BP 72, Châtillon, 92322-France
[b] SIMAP, 1130 rue de la Piscine BP 75, St Martin d'Hères 38402-France

Available online 14 June 2007

Abstract

In order to understand the degradation of thermal barrier coating (TBC) systems better, we determined the adhesion energy (G_c) between the bond coat and the top coat and its evolution during cyclic oxidation. This energy was evaluated by means of a modified four-point bending test. The systems tested consist of a YPSZ (7 wt.%Y_2O_3–ZrO_2) EB-PVD ceramic top coat deposited on a single-crystal AM1 superalloy substrate protected with either a β-(Ni, Pt)Al bond coat or a newly developed Zr-doped β-NiAl bond coat. Although the results show a similar adhesion evolution for both systems, different microstructural degradations are involved.

Keywords: Thermal barrier coatings; Adhesion testing; Cyclic oxidation; Rumpling; Failure mechanisms; Photo-stimulated Luminescence Piezo-Spectroscopy (PLPS)

1. Introduction

Thermal barrier coating (TBC) systems, deposited on superalloy turbine blades, have been developed to allow a significant increase in the combustion gas temperature, and thereby the aircraft engine efficiency. Degradation of these systems results from complex phenomena, linked with the development of the interfacial alumina layer, referred to as the thermally grown oxide (TGO), which eventually lead to the ceramic layer spallation. The comprehensive study of the TBC failure mechanisms, which could provide a reliable lifetime prediction of these systems, has not yet been addressed. Thus, in order to understand the TBC degradation better, a reading of the evolution of their loss of adhesion could be of interest.

This paper presents a monitoring of this evolution made by conducting adhesion tests on as-deposited and oxidised specimens. The systems tested include either a β-(Ni,Pt)Al bond coat or a newly developed Zr-doped β-NiAl bond coat [1]. This Zr-doped bond coat, which presents a very good oxidation behavior, would be an economically interesting alternative to the widely used Pt-modified bond coat as it is processed in fewer steps and contains no Pt. The results of the adhesion tests are discussed in relation with the microstructural evolution observed on oxidised samples. Finally, failure mechanisms of the TBC systems of interest are proposed.

2. Experimental

2.1. TBC Specimen

Plate-shaped thermal barrier coated Ni-based superalloy (sulfur content <0.4 wt. ppm) specimens (60 × 8 × 1 mm) were prepared for the adhesion test. The systems include a 7 wt.% Y_2O_3–ZrO_2 ceramic top coat deposited by EB-PVD (Electron Beam Physical Vapor Deposition) on a single-crystal AM1 superalloy substrate protected with either a β-(Ni, Pt)Al bond coat or a newly developed Zr-doped β-NiAl bond coat. The single crystal substrate faces were oriented along the <001> directions using the back-reflection Laue method. For both bond coats as-deposited aluminium content was equal to 39 at.%.

Thermal cycling exposures were conducted in an automated cyclic furnace at atmospheric pressure. Each cycle is comprised of a 10 min heat up, a 60 min exposure at 1100 °C and a 5 min forced-air cooling down to 200 °C.

The specimens were characterized using field emission gun-scanning electron microscopy equipped with X-ray energy

* Corresponding author. Tel.: +33 146734583; fax: +33 146734164.
E-mail address: pthery@onera.fr (P.-Y. Théry).

0257-8972/$ - see front matter © 2007 Elsevier B.V. All rights reserved.
doi:10.1016/j.surfcoat.2007.06.014

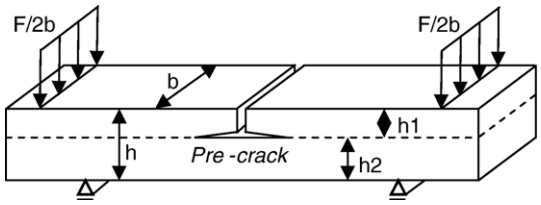

Fig. 1. Four-point bending specimen with symmetrical interfacial cracks [2].

dispersive spectroscopy (FEG-SEM/EDX). The SEM images were analysed using the Aphelion™ software.

2.2. Adhesion test

The adhesion energy of the TBC systems, i.e. the strain energy release rate required for stable crack propagation at the ceramic–substrate interface G_c, was measured by means of a four-point bending test [2] (Fig. 1). This test enables a symmetric crack to propagate from a perpendicular notch along the weakest interface of a multilayer specimen. Between the two inner loading points, stable crack propagation occurs at a constant load. The critical strain energy release rate is derived from this plateau force recorded on the load-deflection curve, without any requirement of crack length measurement.

This well-known adhesion test was adapted to the system of interest, which includes a thin and brittle columnar ceramic layer. This adaptation consists in bonding a stiffening layer to the top of the ceramic layer [3]. This steel layer (AISI 304 L) was bonded using an epoxy adhesive (Araldite® 2011) cured at 100 °C for 30 min. It increases the stored energy in the top layer of the adhesion test specimen and therefore also the driving force for crack propagation. Consequently, the load needed to propagate the interfacial crack becomes smaller. This prevents the ceramic layer and the bond coat, both brittle at room temperature, from cracking and the substrate from yielding [2]. Finally, it simplifies the derivation of the adhesion energy from the experimental force.

The perpendicular notch was machined through the stiffening layer and the top coat at the centre of the specimens using a wire saw (Ø 100 µm) to enable the propagation of the symmetric cracks during the test (Fig. 2).

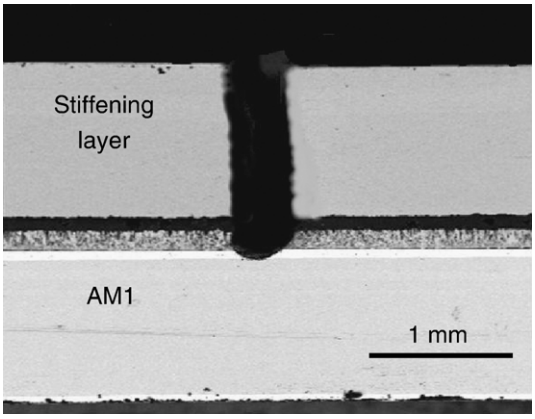

Fig. 2. Partial view of a modified notched four-point bending specimen.

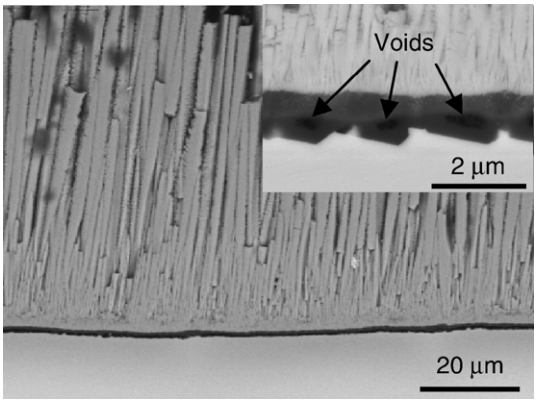

Fig. 3. SEM image of faceted voids developed beneath the alumina scale on a TBC including a (Ni, Pt)Al bond coat which had not been sand-blasted prior to EB-PVD deposition.

As previously mentioned, only stable interfacial crack propagation can give a reading of adhesion energy. A pre-requisite to observing such a stable propagation is the introduction of a pre-crack at the interface. Indeed, without any preset crack source, a large load is needed to initiate the crack and the specimen could consequently be overloaded. In this case, after initiation, catastrophic crack propagation occurs and the force-displacement diagram exhibits no plateau, providing no reliable information on the adhesion energy. A pre-crack was successfully realized by introducing a 1 mm large band at the centre of the specimens which was not sand blasted prior to the EB-PVD

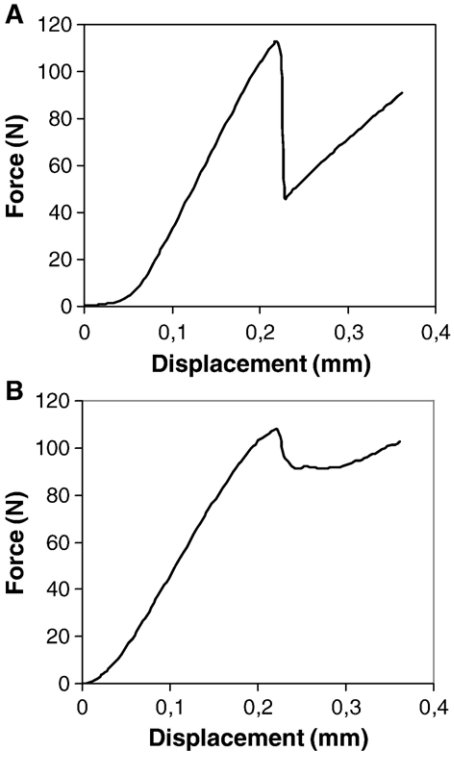

Fig. 4. Force-displacement diagrams recorded during the adhesion test. (A) Without any pre-crack, the specimen is overloaded so that catastrophic crack propagation occurs and the diagram exhibits no plateau. (B) With an efficient pre-crack, stable crack propagation occurs so that the diagram exhibits a plateau.

ceramic deposition, as is usually done. As expected [4], numerous voids, limiting the TBC adherence, were observed at the interface of the band (Fig. 3). During cyclic oxidation a weak alumina scale was retained, so that this area still constituted an efficient pre-crack. Adhesion tests performed on specimens, either pre-cracked or not, demonstrated the pre-crack efficiency (Fig. 4), on as-deposited specimens as well as on oxidised specimens.

The strain energy release rate was derived from the experimental results by means of numerical finite element calculations using the stiffness derivative method [5].

3. Results

3.1. Adhesion energy evolution

The results of the adhesion tests performed on the two TBC systems of interest, as-deposited and oxidised, are summarized in Fig. 5. The results clearly show the effect of cyclic oxidation on the adhesion degradation of the two TBC systems.

The order of magnitude of these values is similar to the one of published results obtained on TBC systems including an air plasma sprayed (APS) top coat [6]. To the authors' knowledge, the only values available for a system including an EB-PVD top coat were reported by H.-A. Bahr et al. [7] (G_c>81 J/m^2 for the as-deposited state and G_c=37 J/m^2 after 10 h at 1100 °C) and A. Vasinonta et al. [8] (G_c=49 J/m^2 for the as-deposited state and G_c=4.3 J/m^2 after 20 h at 1200 °C).

3.2. Fracture surfaces

The fracture surfaces reveal the interface where crack propagation occurred during the adhesion test (Fig. 6). The crack extended along the entire TGO/bond coat interface in the system including the Zr-doped bond coat (Fig. 6.A.), as revealed by the alumina grain imprints, whereas the crack pathway was mixed and complicated in the system including the Pt-modified bond coat (Fig. 6.B.), the crack also going through the TGO or along the TGO/YPSZ top coat interface.

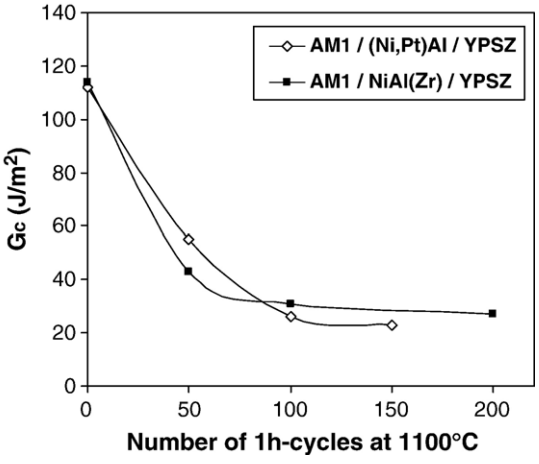

Fig. 5. Adhesion energies G_c of two TBC systems, as a function of the number of 1 h-cycles at 1100 °C. (3 to 5 specimens tested for each result; typical dispersion around 10%).

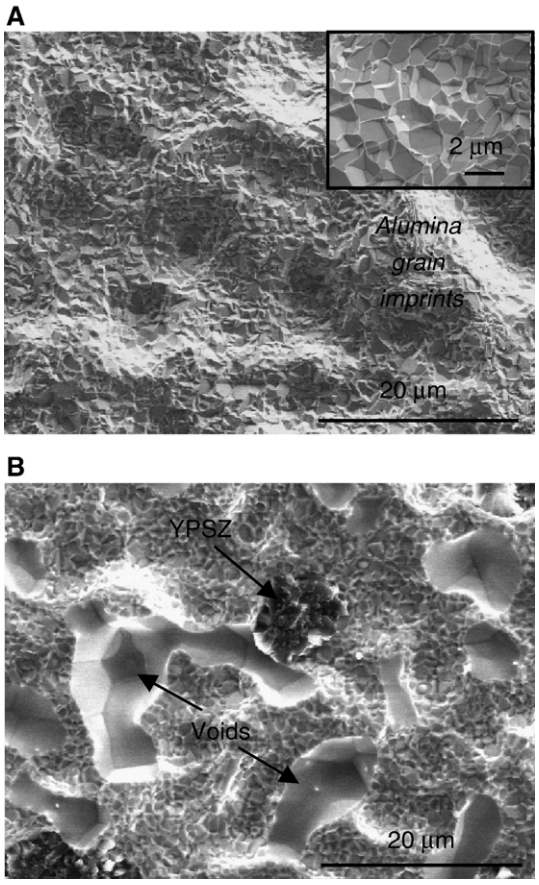

Fig. 6. Fracture surfaces of specimens oxidized 100 1 h-cycles at 1100 °C prior to adhesion test. (A) AM1/β-NiAl(Zr)/YPSZ. (B) AM1/β-(Ni,Pt)Al/YPSZ.

3.3. Bond coat rumpling

Cyclic oxidation resulted in roughening, also termed rumpling [9], of the bond coat on both systems, but to different extents. The evolution of the bond coat surface roughness was evaluated from cross-sectional SEM micrographs, using the arithmetical mean roughness (Ra) measured over a 3 mm length (Fig. 7).

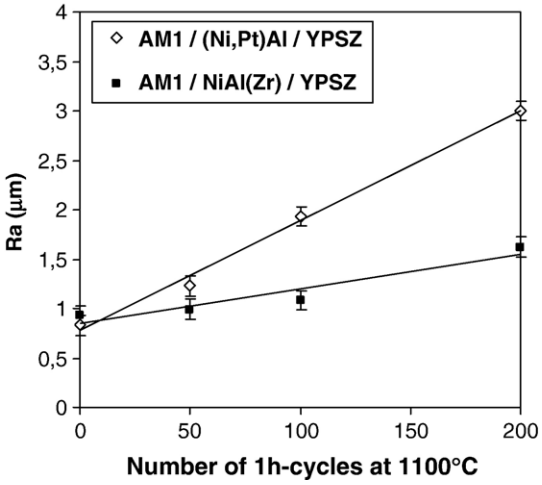

Fig. 7. Arithmetical mean roughness (Ra) of the TGO/bond coat interface of two TBC systems as a function of the number of 1 h-cycles at 1100 °C.

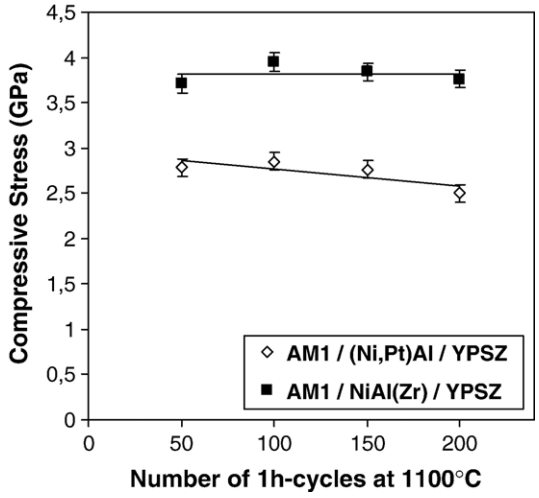

Fig. 8. Evolution of the residual compressive stress in the TGO on two TBC systems as a function of the number of 1 h-cycles at 1100 °C.

3.4. Residual compressive stress in the alumina scales

Residual compressive stress in the TGO was measured by photo-stimulated luminescence piezo-spectroscopy (PLPS) [10] on the oxidised specimens, prior to adhesion testing. The evolution of the residual stress in the TGO on both systems as a function of oxidation cycles at 1100 °C is shown Fig. 8.

4. Discussion

4.1. Evolution of the microstructure and the residual compressive stress in the alumina scales

4.1.1. Interfacial voids

The most noticeable observation on the fracture surfaces is the formation of large interfacial voids on the β-(Ni,Pt)Al bond coat [11,12]. In contrast, no voids were observed on the Zr-doped β-NiAl bond coat. Indeed, such a reactive element doping is known to prevent void formation [13,14].

4.1.2. Bond coat rumpling

The origins of rumpling cannot easily be ascribed to a single phenomenon. Several effects may contribute to the rumpling process [15]. Driven by the highly compressed oxide film, rumpling would be governed by the creep of the bond coat and the mechanical behavior of the TGO. Large stress produced in the bond coat by coating-substrate thermal expansion mismatch and phase transformation, such as the martensitic transformation [16] or the $\beta \rightarrow \gamma'$ transformation [17], may also effectively promote undulation growth.

The slight roughening evolution observed in the Zr-doped bond coat can be attributed to an effect of such a doping on the bond coat creep properties [18] and the TGO mechanical properties [19]. Besides, the martensitic transformation, which occurred in the Pt-modified bond coat, apparently did not occur in the Zr-doped bond coat so that the rumpling promoting stress may be significantly reduced [15].

In addition, the Pt-modified bond coat underwent the $\beta \rightarrow \gamma'$ transformation to a larger extent than the Zr-doped did (Fig. 9).

Aluminium depletion leading to this phase transformation occurred probably more rapidly in the Pt-modified bond coat due to a larger oxide growth rate [20] and an enhancement of aluminium diffusion [21].

4.1.3. Residual compressive stress in the alumina scales

The PLPS measurements clearly demonstrate that the residual stress in the scale is significantly more compressive on the Zr-doped bond coat. Although the change in scale growth mechanism due to reactive element doping was thought to result in lower residual stress [13], these measurements are in accordance with other PLPS measurements conducted on the scale of reactive element containing alloys [22]. This high residual stress might arise from a decrease in the scale creep rate as a result of Zr doping of its grain boundaries [19] and/or the columnar structure of its grains [13].

Due to the progressive rumpling of the bond coat [23], a slight stress relaxation is observed in the scale developed on the Pt-modified bond coat, whereas high compressive stress was maintained during cyclic oxidation in the flat scale developed on the Zr-doped bond coat.

4.2. Adhesion evolution

The adhesion energies measured on the TBC systems of interest, including either a Pt-modified or a Zr-doped β-NiAl bond coat, exhibit a very similar evolution in cyclic oxidation at 1100 °C. For both systems, the as-deposited adhesion is equivalent. Then, it exhibits a sharp drop from 110 J/m^2 down to approximately 50 J/m^2 after the 50 first one-hour cycles at 1100 °C, indicating that the main interface degradations occurred at the beginning of the lifetime of both systems. Finally, a steady state follows until their failure. Although the adhesion energies of both systems vary in the same way, the mechanisms leading to their spallation were found to be different.

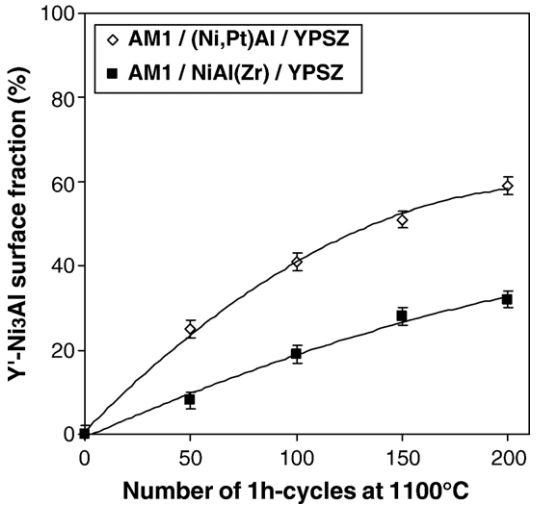

Fig. 9. Evolution of the surface fraction of the γ'-Ni_3Al phase in the bond coats of two TBC systems as a function of the number of 1 h-cycles at 1100 °C.

4.2.1. AM1/β-(Ni, Pt)Al/YPSZ

The adhesion degradation of the TBC system including the Pt-modified β-NiAl bond coat results from two major phenomena. The adhesion is, on the one hand, strongly reduced by the formation of interfacial voids. The important loss of adhesion recorded during the 50 first cycles is consistent with the formation of the voids over this period. Then, the voids continue to grow slowly and their effect is less pronounced. On the other hand, rumpling also greatly contributes to adhesion degradation [24]. Indeed, the bond coat roughness increased continuously during cyclic oxidation so that critical geometrical incompatibilities appeared in the concave regions, which lead to local separations at the TGO/YPSZ top coat interface. Nevertheless, rumpling can also act as a compensatory mechanism, since a convoluted interface can effectively retard an interfacial crack propagation. Thus, no adhesion degradation was recorded over a transient steady state period, before rumpling induced damage reached a critical level and resulted in the TBC spallation.

4.2.2. AM1/β-NiAl(Zr)/YPSZ

In contrast with this well-known failure mechanism, the spallation of the TBC system including the Zr-doped β-NiAl bond coat does not result from voids formation or extensive bond coat roughening. This mechanism was observed on TBC systems including a Pt-modified bond coat which was polished prior to ceramic deposition [25,26]. It is characterized by a flat oxide layer which maintains a high compressive stress throughout the lifetime of the TBC system. This high stress level enables the stored energy in the TGO to significantly build up, especially in the 50 first cycles, and to lead to local separations at the bond coat/TGO interface. These debondings are likely to occur at the crest of surface irregularities where localized normal tensile stresses develop. The adhesion degradation can then stabilize until the stored energy available in the TGO and the top coat is sufficient to drive the TBC failure. Quantitative assessment of the evolution of the stored energy is underway.

5. Conclusion

The adhesion energies of two TBC systems, including either a Pt-modified or a Zr-doped β-NiAl bond coat, were successfully monitored as a function of cyclic oxidation at 1100 °C by means of a test adapted to the system of interest. The similar adhesion evolution measured on both TBC systems indicates that the Zr-doped β-NiAl bond coat constitutes an alternative to the β-(Ni,Pt)Al bond coat.

Nevertheless, different microstructural degradations are involved and the failure mechanisms were eventually found to be different. The failure of the system including the Pt-modified bond coat is mainly due to interfacial voids formation and extensive rumpling of the bond coat. In contrast, in the system including the Zr-doped bond coat, no interfacial voids were observed and the interface remained relatively smooth throughout the lifetime. In this case, the relatively high level of compressive stress in the TGO is most likely responsible for the failure.

Acknowledgment

The authors thank Dr. Terrien from ONERA for his assistance in the PLPS measurements.

References

[1] S. Navéos, G. Oberlaender, Y. Cadoret, P. Josso, M.-P. Bacos, Mater. Sci. Forum 461-464 (2004) 375.
[2] P.G. Charalambides, J. Lund, A.G. Evans, R.M. McMeeking, J. Appl. Mech. 56 (1989) 77.
[3] I. Hofinger, M. Oechsner, H.-A. Bahr, M.V. Swain, Int. J. Fract. 92 (1998) 213.
[4] J.A. Haynes, Scr. Mater. 44 (2001) 1147.
[5] D.M. Parks, Int. J. Fract. 10 (1974) 487.
[6] M. Arai, Y. Okajima, K. Kishimoto, Eng. Fract. Mech. 74 (13) (2007) 2055.
[7] H.-A. Bahr, H. Balke, T. Fett, I. Hofinger, G. Kirchhhoff, D. Munz, A. Neubrand, A.S. Semenov, H.-J. Weiss, Y.Y. Yang, Mater. Sci. Eng., A Struct. Mater.: Prop. Microstruct. Process. 362 (2003) 2.
[8] A. Vasinonta, J.L. Beuth, Eng. Fract. Mech. 68 (2001) 843.
[9] V.K. Tolpygo, D.R. Clarke, Acta Mater. 48 (2000) 3283.
[10] D.R. Clarke, R.J. Christensen, V. Tolpygo, Surf. Coat. Technol. 94-95 (1997) 89.
[11] M.W. Brumm, H.J. Grabke, Corr. Sci. 34 (1993) 547.
[12] D. Zimmerman, M. Bobeth, M. Rühle, D.R. Clarke, in Z. Metallkd., 95, 2, (Carl Hanser Verlag, München, 2004) 84.
[13] B.A. Pint, Oxid. Met. 45 (1/2) (1996) 1.
[14] I.J. Bennett, W.G. Sloof, Mater. High Temp. 20 (3) (2003) 395.
[15] D.S. Balint, J.W. Hutchinson, J. Mech. Phys. Solids 53 (2005) 949.
[16] M.W. Chen, M.L. Glynn, R.T. Ott, T.C. Hufnagel, K.J. Hemker, Acta Mater. 51 (2003) 4279.
[17] V.K. Tolpygo, D.R. Clarke, Acta Mater. 52 (2004) 5115.
[18] C.T. Liu, J.A. Horton Jr., Mater. Sci. Eng., A Struct. Mater.: Prop. Microstruct. Process. 192/193 (1995) 170.
[19] J. Cho, C.M. Wang, H.M. Chan, J.M. Rickman, M.P. Harmer, Acta Mater. 47 (15) (1999) 4197.
[20] B.A. Pint, I.G. Wright, W.Y. Lee, Y. Zhang, K. Prüβner, K.B. Alexander, Mater. Sci. Eng., A Struct. Mater.: Prop. Microstruct. Process. 245 (1998) 201.
[21] Y. Cadoret, D. Monceau, M.-P. Bacos, P. Josso, V. Maurice, P. Marcus, Oxid. Met. 64 (3/4) (2005) 185.
[22] R.J. Christensen, V.K. Tolpygo, D.R. Clarke, Acta Mater. 45 (4) (1997) 1761.
[23] M. Wen, E.H. Jordan, M. Gell, Surf. Coat. Technol. 201 (2006) 3289.
[24] V.K. Tolpygo, D.R. Clarke, K.S. Murphy, Surf. Coat. Technol. 188-189 (2004) 62.
[25] K. Vaidyanathan, E.H. Jordan, M. Gell, Acta Mater. 52 (2004) 1107.
[26] G. Lee, A. Atkinson, A. Selçuk, Surf. Coat. Technol. 201 (2006) 3931.